

TOHOKU EARTHQUAKE: A SURPRISE?

Yan Y. Kagan and David D. Jackson

Department of Earth and Space Sciences, University of California,
Los Angeles, California 90095-1567, USA;

Emails: kagan@moho.ess.ucla.edu, david.d.jackson@ucla.edu

Abstract. We consider three questions related to the 2011 Tohoku mega-earthquake: (1) Why was the event size so grossly under-estimated by Japan’s national hazard map? (2) How should we evaluate the chances of giant earthquakes in subduction zones? and (3) What is the repeat time for magnitude 9 earthquakes off the Tohoku coast? The “maximum earthquake size” is often guessed from the available history of earthquakes, a method known for its significant downward bias. We show that historical magnitudes systematically underestimate this maximum size of future events, but the discrepancy shrinks with time. There are two quantitative methods for estimating the corner magnitude in any region: a statistical analysis of the available earthquake record, and the moment conservation principle. However, for individual zones the statistical method is usually ineffective in estimating the maximum magnitude; only the lower limit can be evaluated. The moment conservation technique, which we prefer, matches the tectonic deformation rate to that predicted by earthquakes with a truncated or tapered magnitude-frequency distribution. For subduction zones, the seismic or historical record is insufficient to constrain either the maximum or corner magnitude. However, the moment conservation principle yields consistent estimates: for all the subduction zones the corner magnitude is of the order 9.0–9.7. Moreover, moment conservation indicates that variations in estimated corner magnitude among subduction zones are

not statistically significant. Another moment conservation method, applied at a point on a major fault or plate boundary, also suggests that magnitude 9 events are required to explain observed displacement rates at least for the Tohoku area. The global rate of magnitude 9 earthquakes in subduction zones, predicted from statistical analysis of seismicity as well as from moment conservation is about five per century – five actually happened.

Short running title: TOHOKU EARTHQUAKE: A SURPRISE?

Key words:

Probability distributions; Seismicity and tectonics; Statistical seismology; Dynamics: seismotectonics; Subduction zones; Maximum/corner magnitude.

1 Introduction

The 11 March 2011 Tohoku, Japan magnitude 9.1 earthquake and the ensuing tsunami near the east coast of Honshu caused nearly 20,000 deaths and more than 300 billion dollars in damage, ranking as one of the worst natural disasters ever recorded (Hayes *et al.*, 2011; Simons *et al.*, 2011; Geller, 2011; Stein *et al.*, 2011). The great difference between the expected and observed earthquake magnitudes contributed to this enormous damage. The estimated maximum magnitude for the Tohoku area (around 7.7) was proposed in the official hazard map (Headquarters for Earthquake Research Promotion, 2005; Seismic Activity in Japan, 2008; Simons *et al.*, 2011).

Several other estimates of the maximum size earthquake in the Tohoku area have been published before 2011. Ruff and Kanamori (1980, Fig. A1) suggested, basing their analysis on historical data, age of subducting plate and plate-rate systematics, that the maximum magnitude is 8.2-8.35. Wesnousky *et al.* (1984, Table 1, Fig. 8) applied the characteristic

earthquake hypothesis to estimate the maximum earthquake size and expected occurrence time for these events in three zones approximately covering the Tohoku earthquake rupture area. Nishenko (1991, Fig. 23 and pp. 234-235) defines the magnitude of characteristic earthquakes in NE Japan, zones $J4 - J6$ as 7.1-7.7. However he does mention an $m8.1$ earthquake in 1611. Minoura *et al.* (2001) suggest that the 869 Jogan earthquake occurred on a fault 240×85 km and was $m8.3$. A similar estimate of the Jogan earthquake magnitude is proposed by Sugawara *et al.* (2012). On the basis of the historical and instrumental catalog analysis, Grunewald and Stein (2006) suggest the maximum magnitude $m8.4$ for the Tokyo area. Koravos *et al.* (2006) provide an estimate $7 < m_{\max} < 8$, based on historical earthquakes since 599 AD, again mentioning a few earthquakes with magnitude slightly larger. Annaka *et al.* (2007) suggest $m_{\max} \approx 8.5$ based on historical earthquakes since 1611. Rikitake and Aida (1988, Table 1, Fig. 5) did not expect the Tohoku area tsunami exceeding 7 m, and defined the maximum magnitude for zones $III - V$ to be within 7.4 – 7.9. “Evaluation of Major Subduction-zone Earthquake(s)” 2008 PDF file at “Seismic Activity in Japan” Japanese Web site (<http://www.jishin.go.jp/main/index-e.html>) defines probabilities of major earthquakes in subduction zones. For the north-east part of Honshu Island, the maximum magnitudes are in the range 6.8-8.2. Nanjo *et al.* (2011) suggest that one should expect magnitudes “up to about 8 or larger for [Japan] offshore events.” These opinions of the Japanese and international researchers confirm that the maximum earthquake size in the Tohoku area was dramatically under-estimated before 2011/03/11.

Several quantitative estimates of the maximum possible earthquakes in the subduction zones had been published before the Tohoku event (Kagan, 1997; Kagan and Jackson, 2000; Bird and Kagan, 2004; McCaffrey, 2007, 2008; Kagan *et al.*, 2010). In these publications, the upper magnitude parameter was determined to be within a wide range from 8.5 to 9.6.

Two quantitative methods have been deployed to estimate the upper magnitude limit: a

statistical determination of the magnitude–moment/frequency parameters from earthquake data alone, and a moment conservation principle in which the total moment rate is estimated from geologic or geodetic deformation rates (Kagan, 1997).

The distinction between maximum and corner magnitudes refers to different approaches in modeling the magnitude-frequency relationship for large earthquakes. In one approach, the classical Gutenberg-Richter magnitude distribution is modified by truncating it at an upper limit the “maximum magnitude.” In another approach, an exponential taper is applied to the moment distribution derived from the classical magnitude distribution. For the tapered Gutenberg-Richter (TGR) distribution the “corner moment” is the value at which the modeled cumulative rate is reduced to $1/e$ of the classical rate, and the “corner magnitude” is that which corresponds to the corner moment. In either approach, the rate of earthquakes of any magnitude and the total seismic moment rate can be computed from three observable parameters: the rate of earthquakes at the lower magnitude threshold, the “ b -value” or asymptotic slope of the magnitude distribution, and the maximum or corner magnitude. Conversely, the maximum or corner magnitude may be determined if the threshold rate, b -value, and total moment rate are known.

We generally shun the use of “maximum magnitude” because there is no scientific evidence that it really represents a maximum possible magnitude, although it is frequently interpreted that way. Where the two approaches lead to similar conclusions, we’ll generalize the discussion by referring to the “upper magnitude parameter.”

Below we use the term m_{\max} to signify the upper limit of the magnitude variable in a likelihood map or the limit of integration in an equation to compute a theoretical tectonic moment arising from earthquakes. As we will see below, in different approximations of earthquake size distribution, m_{\max} may have various forms, though their estimated numerical values are usually close. We do not treat m_{\max} as a firm limit, but we use it as a convenient

general reference because many other researchers do so.

The statistical estimate of the maximum magnitude for global earthquakes, including subduction zones and other tectonic regions, yielded the values $m_{\max} \approx 8.3$ (Kagan and Jackson, 2000). The moment conservation provided an estimate for subduction zones $m_{\max} = 8.5 - 8.7 \pm 0.3$ (Kagan, 1997; 2002b). Moreover, the maximum earthquake size was shown to be the indistinguishable, at least statistically, for all the subduction zones studied. Applying a combined statistical estimate and moment conservation principle, Bird and Kagan (2004) estimated the corner magnitude to be about 9.6. As we explain below, the difference between the above estimates (8.6 *vs* 9.6) is caused mainly by various assumptions about the tectonic motion parameters. These m_{\max} determinations, combined with the observation of very large ($m \geq 9.0$) events in the other subduction zones (Stein and Okal, 2007, 2011; McCaffrey, 2007, 2008), should have warned of such a possible earthquake in any major subduction zone, including the Sumatra and Tohoku areas.

In Section 2 below we consider two statistical distributions for the earthquake scalar seismic moment and statistical methods for evaluating their parameters. Section 3 discusses the seismic moment conservation principle and its implementation for determining the upper magnitude parameter. We then demonstrate how these techniques for size evaluation work in subduction zones, showing that $m_{9.0} - m_{9.7}$ earthquakes can be expected in all major zones, including the Tohoku area. For the Tohoku area the approximate recurrence interval for $m \geq 9.0$ earthquake is on the order of 350 years (Kagan and Jackson, 2012, see more in the Discussion Section). By the term ‘recurrence interval’ we do not imply that large earthquakes occur cyclically or quasi-periodically; contrary to that we presented an evidence that all earthquakes including the large ones are clustered in time and space (Kagan and Jackson, 1999, see also the Discussion Section).

2 Evaluation of earthquake size distribution for subduction zones

2.1 Earthquake catalogs

We studied earthquake distributions and clustering for the global CMT catalog of moment tensor inversions compiled by the GCMT group (Ekström *et al.*, 2005; Ekström, 2007; Nettles *et al.*, 2011). The present catalog contains more than 33,000 earthquake entries for the period 1977/1/1 to 2010/12/31. The event size is characterized by a scalar seismic moment M .

We also analyzed the Centennial (1900-1999) catalog by Engdahl and Villaseñor (2002). The catalog is complete down to magnitude 6.5 (M_S/m_B or their equivalent) during the period 1900-1963 and to 5.5 from 1964-1999. Up to 8 different magnitudes for each earthquake are listed in the catalog. We use the maximum of the available magnitudes in the Centennial catalog as a substitute for the moment magnitude and construct a moment-frequency histogram. There are 1623 shallow earthquakes in the catalog with $m \geq 7.0$; of these 30 events have $m \geq 8.5$.

2.2 Seismic moment/magnitude statistical distributions

In analyzing earthquakes here, we use the scalar seismic moment M directly, but for easy comparison and display we convert it into an approximate moment magnitude using the relationship (Hanks, 1992)

$$m_W = \frac{2}{3}(\log_{10} M - C), \quad (1)$$

where $C = 9.0$, if moment M is measured in Newton m (Nm), and $C = 16.0$ for moment M expressed in *dyne-cm* as in the GCMT catalog. The equation above provides a unique mapping from magnitude to moment, so where appropriate we'll use both of the same subscripts.

Thus m_{\max} implies a corresponding M_{\max} , etc.

Since we are using the moment magnitude almost exclusively, later we omit the subscript in m_W . Unless specifically indicated, we use for consistency the moment magnitude calculated as in (1) with the scalar seismic moment from the GCMT catalog.

In this work we consider two statistical distributions of the scalar seismic moment: (a) the truncated Gutenberg-Richter (G-R) or equivalently truncated Pareto distribution, in which the upper magnitude parameter is the maximum magnitude, and (b) the gamma distribution (Kagan, 2002a; 2002b), in which the upper magnitude parameter is the corner magnitude m_{cg} .

For the truncated Pareto distribution the probability density (pdf) is

$$\phi(M) = \frac{M_{xp}^\beta M_t^\beta}{M_{xp}^\beta - M_t^\beta} \beta M^{-1-\beta} \quad \text{for } M_t \leq M \leq M_{xp}. \quad (2)$$

Here M_{xp} is the upper truncation parameter, M_t is the lower moment threshold (the smallest moment above which the catalogue can be considered to be complete), β is the index parameter of the distribution. Note that $\beta = \frac{2}{3}b$, where b is the familiar b -value of the Gutenberg-Richter distribution (Gutenberg and Richter, 1954, pp. 16-25).

The gamma distribution has the pdf

$$\phi(M) = C^{-1} \frac{\beta}{M} (M_t/M)^\beta \exp[-(M_t - M)/M_{cg}], \quad \text{for } M_t \leq M < \infty, \quad (3)$$

where M_{cg} is the corner moment parameter controlling the distribution in the upper ranges of M ('the corner moment') and C is a normalizing coefficient. Specifically,

$$C = 1 - (M_t/M_{cg})^\beta \exp(M_t/M_{cg}) \Gamma(1 - \beta, M_t/M_{cg}), \quad (4)$$

where Γ is the gamma function (Bateman and Erdelyi, 1953). For $M_{cg} \gg M_t$ the coefficient $C \approx 1$. Below we simplify the notation M_{px} and M_{cg} as M_x and M_c , respectively, keeping

the notation M_{\max} to represent either M_{px} or M_{cg} as appropriate. Thus, each distribution is controlled by two parameters: its slope for small and moderate earthquakes, β , and its maximum or corner moment M_x or M_c describing the behavior of the largest earthquakes. The two equations above are normalized distributions. Both need a multiplicative constant, the threshold earthquake rate, to calculate rates at any magnitude above the threshold.

In Fig. 1 we show the magnitude-frequency curves for shallow earthquakes (depth less or equal to 70 km) in the Japan-Kurile-Kamchatka #19 Flinn-Engdahl (Flinn *et al.*, 1974; Young *et al.*, 1996) zone for the period 1977-2010 (i.e., before the Tohoku event). Similar curves for period before and after 2011/1/1 for the rupture zone of the Tohoku earthquake are shown in our companion paper (Kagan and Jackson, 2012, Figs. 1, 2). Knowing the distribution of the seismic moment, one can calculate occurrence rates for earthquakes of any size, so we need a reliable statistical technique to determine the parameters of a distribution.

2.3 Likelihood evaluation of distribution parameters

We applied the likelihood method to obtain estimates of β and m_c (Kagan, 1997, 2002a). Fig. 2 displays the map of the log-likelihood function for two parameters of the gamma distribution. The β -value (around 0.61 ± 0.038) can be determined from the plot with sufficient accuracy (Fig. 2), but the corner magnitude evaluation encounters serious difficulties. The upper contour of the 95% confidence area in the likelihood map is not well-constrained and allows infinite M_x . This means that only the lower limit for m_c , around 8.2, can be reliably evaluated with the available data. Hence the maximum likelihood estimate ($m_c = 8.7$) is not well-constrained by the likelihood map. However, even the lower limit for m_c is higher than the maximum magnitude size ($m7$ to $m8$) proposed by the official hazard map for the Tohoku area (Headquarters for Earthquake Research Promotion, 2005; Seismic Activity in Japan, 2008; Simons *et al.*, 2011). Thus, a simple statistical test could have revealed that

earthquakes much larger than magnitude 7 to 8 should be expected.

Fig. 2 is similar to the likelihood map constructed by Bird and Kagan (2004, Fig. 7F; see also Table 5) for all subduction zones taken together. The calculation in that plot was made with the tapered G-R distribution (TGR) discussed by Kagan (2002a). That distribution is similar in spirit to the gamma distribution, except that the taper is applied to the cumulative rather than the density distribution. For $\beta = 0.64$ and identical total moment rates, the m_c -values of the TGR are 0.39 lower than those for the gamma distribution (Kagan, 2002b; see also Kagan and Jackson, 2000, Fig. 2 and its discussion).

From Bird and Kagan’s map (2004, Fig. 7F), the lower limit for m_{cm} is about 9.0, but even the complete 20-th century earthquake record is insufficient to obtain the upper statistical limit. Kagan (1997) has showed that all subduction zones have essentially the same maximum magnitude parameters; this result implies that the corner magnitude m_{cg} is at least 9.4 in the major zones.

Geller (2011) and Stein *et al.* (2011) suggest that a major reason for grossly underestimating the maximum magnitude for Japanese earthquakes is that many seismologists accept the flawed seismic gap model based on the characteristic earthquake hypothesis (see, for example, Wesnousky *et al.*, 1984; Annaka *et al.*, 2007, and the Introduction Section). This inadequate model suggests that a fault can be subdivided into segments and a maximum allowable event on such a segment is limited either by its length or by the available historic or instrumental record. Bird (2010) found that even “diligent and extensive mapping of faults [cannot] provide reliable estimates of the expected maximum earthquakes at these faults”. Kagan and Jackson (1991) reported serious problems with the seismic gap model. Jackson and Kagan (2011) summarize theoretical and observational arguments against the seismic gap/characteristic earthquake model. Simons *et al.* (2011, p. 1425) also present some evidence contradicting this hypothesis, indicating that historical events do not repeat one

another and their slip may change significantly. They conclude “the concept of a characteristic subduction earthquake with approximately the same slip per event at a given location may be of limited use”.

3 Seismic moment conservation principle

We try to estimate the upper bound of the seismic moment-frequency relation, using the moment conservation principle as another, more effective method for determining the maximum/corner magnitude. Quantitative plate tectonics and space geodetic methods currently provide a numerical estimate of the tectonic deformation rate for all major tectonic plate boundaries and continental regions of significant distributed deformation (Bird and Kagan, 2004; Kagan *et al.*, 2010). We compare these estimates with a similar one for the seismic moment release.

The seismic moment rate depends on three variables (see Eqs. 6, 7 below) –

- 1. The number of earthquakes in a region (N),
- 2. The β -value (or b -value) of the G-R relation,
- 3. The value of the maximum (corner) magnitude m_c .

The tectonic moment rate \dot{M}_T depends on the following three variables which are not well-known –

- 1. The seismogenic zone width (W – 30-104 km),
- 2. The seismic efficiency (coupling) coefficient (χ – 50-100%),
- 3. The value of the shear modulus (μ – 30-49GPa).

$$\dot{M}_T = \chi \mu W \mathcal{L} \dot{u}, \quad (5)$$

where \dot{u} is the slip rate, \mathcal{L} is the length of a fault (compare Eq. 13 by Kagan, 2002b).

3.1 Area-specific conservation principle

The discussion in this Subsection is based generally on our previous papers (Kagan, 2002a; 2002b). In those papers we consider two theoretical moment-frequency models: (a) a truncated Pareto distribution;

$$\dot{M}_s = \frac{\alpha_0 M_0^\beta \beta}{1 - \beta} M_x^{1-\beta} \xi_p, \quad (6)$$

where \dot{M}_s is the seismic moment rate and α_0 is the rate of occurrence for events with moments larger or equal M_0 ; $\alpha_0 = N/\Delta T$ with ΔT as the catalog duration. In most cases M_0 can be chosen to correspond to the observational threshold moment M_t . Coefficient ξ is a correction factor needed if the distribution is left-truncated close to the maximum or the corner moment; under usual circumstances it equals 1.0. For the gamma distribution (b) the analogous formula is

$$\dot{M}_s = \frac{\alpha_0 M_0^\beta \beta}{1 - \beta} M_c^{1-\beta} \Gamma(2 - \beta) \xi_g. \quad (7)$$

We assume that the two theoretical laws (Eqs. 6 and 7) describe a distribution with the same moment rate \dot{M}_s and seismic rate of occurrence α_0 . Using Eqs. 6 and 7, relations between the maximum or corner moments can be specified

$$M_{xp} \beta^{1/(1-\beta)} = M_{cg} [\beta \Gamma(2 - \beta)]^{1/(1-\beta)}. \quad (8)$$

The gamma function $\Gamma(2 - \beta)$ changes slowly in the range of β -values encountered in the moment-frequency relations: for values of β in the interval 1/2 to 2/3, the gamma function is $\Gamma(2 - 1/2) = 0.886$ or $\Gamma(2 - 2/3) = 0.893$. Therefore, the difference between the maximum and corner magnitudes is relatively small: for southern California our calculations (Kagan, 2002b, Fig. 2) yield the magnitude values $m_x = 8.35$, and $m_c = 8.45$ for the two distributions shown in Eqs. 2 and 3.

Fig. 3 shows the β -values determined for 18 Flinn-Engdahl (FE) zones (Gutenberg and Richter, 1954, Fig. 1; Flinn *et al.*, 1974; Young *et al.*, 1996) listed in sequential order. These FE regions correspond to major subduction zones and they have been selected by us because the FE regionalization had been defined before the GCMT catalog started, thus eliminating selection bias. It is also easier to replicate our results (the programs and tables for the Flinn-Engdahl zones are publicly available, see Section ‘Data and Resources’). In this plot we use the GCMT catalog at the same temporal interval as in our previous paper (Kagan, 1997). In Fig. 4 the catalog duration is extended to the end of 2010. Both plots demonstrate that (a) the β -values do not depend significantly on the catalog duration, though their standard errors do decrease with the duration and earthquake numbers increase; (b) the β -values are approximately the same for all the zones, and the hypothesis of the values equality cannot be statistically rejected (Kagan, 1997). The additional data since 1995 makes the argument for a common β much stronger.

Figs. 5, 6, and 7 show the distribution of the corner magnitude obtained, using Eq. 7, for the earthquake catalogs of different time duration. Estimates of m_c for all diagrams in all the subduction zones are statistically indistinguishable. This means that all such zones should have the same maximum or corner magnitude.

The estimate of m_c depends on the parameter value used to calculate the tectonic moment rate (Eq. 5): for $\beta = 2/3$, the change of any parameters (such as W or χ) by a factor of two implies an increase or decrease of the m_c by about 0.6 (Kagan, 2002b, Eq. 17). We see this influence by comparing Table 1 with results for the subduction zones in similar Table 1 by Kagan (1997), where the parameters used for calculating tectonic rate were $W = 30$ km, $\mu = 30$ GPa, $\chi = 1.0$. The difference in the m_c estimates for the two tables is caused mainly by changes in the above parameters.

We also compare the m_c -values for the same zones in Figs. 5, 6, and 7. The values in

Figs. 6 and 7 differ greatly: by 0.5 and more in five zones: Kermadec, Fiji, Japan-Ryukyu, Sunda, and Andaman (FE12, 13, 20, 24, 46). This is not surprising since the magnitudes in the Centennial catalog were determined with large random and systematic errors. In addition, given the high magnitude threshold, the earthquake numbers will have significant random fluctuations. When matching up Figs. 5 and 6, only one zone, Andaman-Sumatra, shows a m_c difference of about 0.9. This finding is due to the 2004 Sumatra earthquake and its aftershocks which significantly increased the total number of events to 143 in 34 years (Table 1) *versus* 22 earthquakes in 19.5 years in Table 1 by Kagan (1997). The annual rate increase is by a factor 3.15, which for $\beta = 2/3$ corresponds to m_c decrease of 1.0. In our m_c calculations (Eq. 7) we use the β -values determined for each zone.

As mentioned, the hypothesis that the m_c -values are the same within their uncertainties for all subduction zones considered cannot be rejected with statistical significance. Thus, the conjecture that $m_c \approx 9.0 - 9.7$ in all such zones is supported by comparing the theoretical estimates with measured magnitude values in several subduction zones. For example, a $m9.0$ earthquake occurred in zone #19 (Kamchatka, Russia) on November 4, 1952, confirming that this subduction zone could experience large earthquakes beyond $m9$.

In Table 1) we also calculate parameter values for the Tohoku area (latitudes $35 - 40^\circ\text{N}$, longitudes $140 - 146^\circ\text{E}$). The length of this trench zone is around 620 km in this spherical rectangle. The value of the tectonic moment accumulation rate attributed to the subducting Pacific plate is compatible with that proposed by Ozawa *et al.* (2011) in the Japan trench area from latitude 36°N to 39.5°N (1.63×10^{20} Nm/y). Ozawa *et al.* (2011) also suggest using $\mu = 40$ GPa for the Japan trench.

Whereas the values of the parameters β and m_c are approximately the same for the Tohoku area and Flinn-Engdahl zone #19, other entries for these rows (12 and 12a) differ significantly. This means that the maximum observed earthquake or the ratio of the seismic

rate to tectonic rates (ψ) for individual subduction zones varies greatly and cannot be used reliably to characterize area seismicity.

For about 110 years of the instrumental seismic record, five zones have experienced earthquakes with a magnitude 9 or larger. Figs. 5–7 also show that for the longer catalog, the average maximum observed magnitude approaches the average estimate of m_c . This suggests that if the available earthquake record duration were comparable to the recurrence time of the largest earthquakes (a few hundred years), the difference between the observed maximum magnitude (m_o) and m_c would largely disappear.

Using the parameter values for the moment-frequency distribution determined by Bird and Kagan (2004, Table 5) for all the subduction zones ($b = 0.96$, $M_t = 3.5 \times 10^{17}$ Nm, $\alpha_t = 76.74$ eq/y, $m_c = 9.58$), we calculate the number of $m \geq 9$ events expected to occur worldwide over a century

$$N(m > 9) = 100.0 \times \alpha_t \times 10^{-0.96(9.0 - 5.696)} = 5.2. \quad (9)$$

In fact five large earthquakes with magnitude 9 or greater did occur in the last 100 years (see Figs. 5–7). The distribution parameters (Bird and Kagan, 2004) were estimated before two recent giant earthquakes struck, so the almost perfect correspondence can be considered a coincidence.

Fig. 8 again demonstrates how the catalog duration affects the ratio of the seismic rate to the tectonic rate for different subduction zones. That ratio is below one for a shorter catalog, but increases to a value close to 1.0 for a longer list. This increase is caused mainly by a few large earthquakes that struck South America and Sumatra regions. As Zaliapin *et al.* (2005) show, a sum of the scalar earthquake moments varies widely due to their power-law distribution.

3.2 Geometric self-similarity of earthquake rupture

Fig. 9 displays an update of Fig. 6a by Kagan (2002c). Several recent mega-earthquakes are included in the plot: the 2004 Sumatra ($m9.1$) and the Tohoku ($m9.2$) events – the right-hand symbols in the diagram, as well as preliminary results for two 2012/04/11 strike-slip earthquakes off the Sumatra coast (McGuire and Beroza, 2012). As mentioned below Eq. 1, for all earthquake magnitudes we apply (1) to the available GCMT scalar moment. Despite the differences in the aftershock zone lengths for the Sumatra and the Tohoku events, emphasized in many publications, the symbols for these earthquakes on the graph are not far away. The vertical difference is smaller than the scatter for moderate earthquakes. The seeming contradiction of their size evaluation is caused by various techniques employed in measuring the rupture size. We use the same measurement method for all earthquakes: namely, a fit of the aftershock spatial scatter by a two-dimensional Gaussian distribution (Kagan, 2002c). For Sumatra and Tohoku events we obtain the aftershock zone size ($2 \times \sigma$ confidence area length) 905 and 533 km, respectively. Two major strike-slip events off the Sumatra coast ($m8.6$ and $m8.3$, shown by ‘+’ symbols in the plot) are only slightly above the regression line for all earthquakes, thus they follow a common relation between the earthquake size and the length of aftershock zone.

Comparing the regression results from Fig. 9 with those of Fig. 6a by Kagan (2002c) demonstrates that the scaling parameter estimates are robust. Since 2000 these earthquake numbers have increased by almost a factor of two. Moreover, in Fig. 9 there are three major ($m \geq 8.8$) events, whereas the largest earthquake in the 2002 study was $m8.4$. However, the values of regression coefficients in both datasets are essentially the same.

Fig. 9 shows both linear and quadratic regression curves for log length versus magnitude. There is practically no difference between linear and quadratic fits. No observable scaling

break or saturation occurs for the largest earthquakes of different focal mechanisms; thus, the earthquake geometrical focal zones are self-similar. Assuming self-similarity, we adopted the following scaling for the average length (L), the average downdip width (W), and the average slip (U) as a function of the moment (M): the length (L) is proportional to the cube root of the moment: $L \propto \sqrt[3]{M}$, implying a self-similarity of the earthquake rupture pattern, i.e., W and U are also proportional to $\sqrt[3]{M}$. The average slip is proportional to the average length implying nearly constant value for stress/strain drop which is related to U/L .

The above results imply that the earthquake slip penetrates well below the seismogenic layer during large earthquakes. Shaw and Wesnousky (2008) and McGuire and Beroza (2012) also note that significant coseismic slip occurs below the seismogenic layer. If the downdip seismogenic width W changes for the largest earthquakes, it may influence the calculation of tectonic rate \dot{M}_T (see Eq. 5).

3.3 Conservation principle for faults

Here we consider moment conservation in the specific case that tectonic deformations are dominated by a fault or plate boundary with estimated slip rate. For simplicity we'll refer to plate boundary surfaces as faults.

Many attempts have been made to compare the slip budget at a subduction zone with its release by earthquakes. McCaffrey (2007, 2008) compared the slip values at the global subduction zones with their release by earthquakes spanning the whole length of a zone. He found that for practically for all the zones, $m9$ and greater earthquakes are possible with recurrence times on the order of a few centuries.

In particular, for Japan McCaffrey (2008) calculated the maximum moment M_{\max} as

$$M_{\max} = \mu \bar{u} L Z_{\max} / \sin \delta, \quad (10)$$

where \bar{u} is the average slip, Z_{\max} is the maximum depth of the slip (40 km used), and δ is the average fault dip angle (taken to be 22° for Japan), implying $W = 106.8$ km. The recurrence time for the maximum earthquake is

$$T = \bar{u} / f \chi \nu, \quad (11)$$

where ν is the plate motion rate, f is the fraction of the total seismic moment in m_9 earthquakes, and $\bar{u} = 2.5 \times 10^{-5} L$. The parameter f is taken to be equal to $1 - \beta$ (apparently using results for the characteristic earthquake distribution by Kagan, 2002a; 2002b). By taking $L = 654$ km, $\beta = 0.57$, $\nu = 62 - 81$ mm/y, and $\chi = 1$, McCaffrey obtains $M_{\max} = 10^{22.53}$ Nm, i.e., $m_{\max} = 9.0$, and $T \approx 532$ y.

Simons *et al.* (2011) considered how the slip in the Tohoku area on the order $\nu = 80 - 85$ mm/y is accommodated by subduction earthquakes. They proposed that only very large events, similar to the Tohoku $m_{9.2}$ earthquake, can explain this displacement rate. Simons *et al.* (2011) included only the largest earthquakes in the slip budget. However, events smaller than the maximum earthquake also contribute to the slip budget, and all earthquakes need to be considered in boundary-specific calculations.

A discussion in this Subsection is based broadly on one of our previous papers (Kagan, 2005). Several issues need to be noted in fault-specific slip calculations:

- 1. The form of the general (area-specific) distribution of earthquake sizes. To simplify calculations we take it as the truncated Pareto distribution (see Eq. 2).
- 2. The fault-specific moment distribution – large earthquakes have a bigger chance to intersect a surface; hence the moment distribution differs from area-specific concerns.
- 3. The geometric scaling of earthquake rupture. As described earlier, length-width-slips are scale-invariant, i.e., for an earthquake of magnitude m : $L_m, W_m, u_m \propto \sqrt[3]{M}$.
- 4. Geometric self-similarity of earthquake rupture implies that the earthquake depth

distribution would differ for small versus large shocks: at least for strike-slip earthquakes, large events would penetrate below the seismogenic layer. For thrust and normal events, the consequences of geometric self-similarity are not clear; their depth distribution has not been sufficiently studied.

- 5. Most small earthquakes do not reach the Earth’s surface and therefore do not contribute to surface fault slip. The contribution of small earthquakes needs to be properly computed.

Because the distribution of slip with depth is poorly understood, we calculate the maximum earthquake size for several special simple cases. An earthquake of moment M (magnitude m) is specified as

$$M = \mu L_m W_m \bar{u}_m. \quad (12)$$

Using the results shown in Fig. 9, we presume for an earthquake of magnitude $m = 7.0$ or moment $M = 10^{19.5}$ Nm, that $L_7 = 60$ km, $W_7 = 10$ km, and $\bar{u}_7 = 1.76$ m or $\bar{u}_7 = 1.076$ m, depending on the value of the shear modulus: $\mu = 30$ GPa or $\mu = 49$ GPa, respectively.

Slip distribution over the fault plane is highly non-uniform in a horizontal direction (Manighetti *et al.*, 2005, 2009). Kagan (2005, [51]) argued that ‘the slip of large earthquakes should “catch up” with the slip deficit at the Earth’s surface left by smaller events’. Thus, the slip of large events must be larger at the surface than in the middle of a seismogenic zone. Fialko *et al.* (2005) and Kaneko and Fialko (2011) show several examples of $m7$ earthquakes which exhibit a strong slip deficit close to the Earth’s surface. This may imply that the seismic efficiency coefficient (χ) may also change with depth. However, since we lack reliable data, for our approximate calculations, we take slip to be uniform over a rectangle $L_m \times W_m$.

We specify earthquake magnitude m rupture dimensions as

$$L_m = L_7 \times \left(10^{1.5m+9} / 10^{19.5} \right)^{1/3}. \quad (13)$$

Analogous expressions are used for W_m and \bar{u}_m .

The relationship between surface slip and the maximum earthquake size depends on the extent to which earthquakes of a given size break the surface. We consider below three special cases. In the first, we assume earthquakes of all sizes are uniformly distributed on the fault surface. In the second, we assume all earthquakes larger than a given magnitude, and only those, break the surface. In the third, we assume that small earthquakes are uniformly distributed above a given depth, but larger ones may penetrate deeper.

In the first simple case of the maximum earthquake size calculation, we suppose that earthquakes of all sizes are distributed uniformly over a fault surface of width W . Then, as we mentioned above, for an earthquake with magnitude m , the surface slip contribution u'_m would be

$$u'_m = u_m \times W_m/W \quad \text{for} \quad W \geq W_m, \quad (14)$$

accounting for the fact that only a few of the smaller earthquakes would reach the surface.

In deriving formulas for boundary-specific surface displacement U_s , we simplify Kagan's (2005) results, taking into account the self-similarity of earthquake rupture (13)

$$U_s = \frac{\lambda_m u'_m L_m}{1.5 - b}, \quad (15)$$

where $\lambda_m = \alpha_m/\mathcal{L}$ is the rate of earthquakes with magnitude greater or equal m per km of a fault surface. If $W_m = W$ is due to assumed scaling, the resulting U_s would always be the same, since an increase in u_m and L_m would be compensated by a decrease in λ_m .

Making some order-of-magnitude calculations, we estimate the slip rate for the Tohoku area. If the magnitude is not close to the maximum, α_m scales with magnitude m as $10^{b(7-m)}$ (see Eq. 2). Thus, from Fig. 1 the annual rate of $m \geq 5.8$ earthquakes is 425/34, and $\beta = 0.61$. Hence $\alpha_7 = (425/34) \times 10^{-0.61 \times 1.5 \times 1.2} = 0.997 \simeq 1.0$ and $\mathcal{L} = 3,000$ km. Then for $b = 1$ and $m = 7$ we obtain $U_s = 7$ mm/y. For $m = 8$ the slip rate is $U_s = 22$ mm/y, and

$U_s = 70$ mm/y for $m = 9$. If we replace $\mu = 30$ GPa by $\mu = 49$ GPa, then for $m = 9$ the slip is $U_s = 43$ mm/y. All these values are smaller than $U_s = 82.5$ mm/y suggested by Simons *et al.* (2011) for the Tohoku area. Therefore, the results do not support this case of fault surface slip distribution, unless the present rate of $m5.8$ and larger earthquakes is below the long term average.

For the second case we presume that all surface slip is due to earthquakes exceeding a certain size (m_f) which always rupture the Earth's surface. In effect, we suppose that small earthquakes do not contribute to the surface slip. Such a model may be appropriate for strike-skip faults like those in California, where very few small events occur near the surface (Kagan, 2005). It is possible that even for subduction zones, this model would produce more correct results.

Then for $b \neq 1.0$ we obtain

$$U_s = \frac{\lambda_f u_f L_f}{1.0 - b} \times [10^{(b-1.0)(m_x - m_f)} - 1], \quad (16)$$

and for $b = 1$

$$U_s = \lambda_f u_f L_f \log 10 \times (m_x - m_f). \quad (17)$$

Several calculations can be made with these formulas to get a rough estimate of the maximum magnitude m_x needed to obtain the slip rate $U_s = 82.5$ mm/y. For $b = 1$ and $\mu = 30$ GPa, $m_x = m_f + 1.02$. Therefore, if we assume $m_f = 7.0$, $m_x = 8.02$ and for $m_f = 8.0$, as more appropriate for subduction zones, $m_x = 9.02$. These values depend, of course, on the presumed parameters of the earthquake rupture. If we take the values $L_7 = 37.5$ km, $W_7 = 15$ km, and $\bar{u}_7 = 1.87$ m, as suggested by Kagan (2005), the estimate of the maximum magnitude changes to $m_x = m_f + 1.53$. A similar increase of m_x occurs if we modify μ : for $\mu = 49$ GPa, $m_x = m_f + 1.65$. If we change the b -value, for instance, take $b = 0.9$, but keep $\mu = 30$ GPa, then $m_x = m_f + 0.91$.

For the third case, we consider a combination of two models (Eqs. 15 and 17): we suppose that in the upper part of the fault surface with the width W_f , small earthquakes are distributed uniformly, whereas large earthquakes $m \geq m_f$ penetrate deeper. Thus, the total slip would be a sum of two terms: one reflecting the contribution of small and moderate events and the other from large earthquakes. Then taking $b = 1$, $m_f = 8$, $W_f = 31.6$ km, and $\mu = 49$ GPa, we obtain $m_x = 8.79$.

Calculations in this Section are more subjective than those in the previous Subsection 3.1; unfortunately the distributions of the slip and the earthquake depth have not yet been studied as thoroughly as the area-specific magnitude-frequency relation. However, these approximate computations imply that the maximum magnitude in the Flinn-Engdahl zone #19 and in the Tohoku area is around 9.0, i.e., much greater than was assumed in the various hazard maps for Japan compiled by many investigators (see the Introduction).

4 Discussion

It is commonly believed that after a large earthquake, its focal area “has been de-stressed” (see, for example, Matthews *et al.*, 2002), thus lowering the probability of a new large event in this place, though it can increase in nearby zones. This reasoning goes back to the flawed seismic gap/characteristic earthquake model (Jackson and Kagan, 2011). Kagan and Jackson (1999) showed that earthquakes as large as 7.5 and larger often occur in practically the same area soon after a previous event. Michael (2011) shows that earthquakes as large as $m8.5$ are clustered in time and space: thus, such a big event does not protect its focal area from the next giant shock.

Any forecast scheme that extrapolates the past instrumental seismicity record would predict future moderate earthquakes reasonably well. However, as the history of the Tohoku

area shows, we need a different tool to forecast the largest possible events. In our forecasts we consider the earthquake rate to be independent of the earthquake size distribution, so the latter needs to be specified separately.

Why is it so difficult to determine the maximum earthquake size for each subduction zone and its recurrence period? This question is especially important after two unpredicted giant earthquakes: the 2004 Sumatra and the 2011 Tohoku. Our available earthquake record is so short that it is difficult to obtain this information by simple observation.

As indicated earlier, the seismic moment conservation principle can answer our questions. The general idea of moment conservation was suggested some time ago (Brune, 1968; Wyss, 1973; Molnar, 1979; Anderson, 1979). However, without knowledge of the earthquake size distribution, calculating the rate of huge earthquakes leads to uncertain or contradictory results. The classical G-R relation is not helpful in this respect because it implies infinitely large earthquakes. Only a modification of the G-R law that limits the upper moment can provide a tool to match earthquake and moment rates. Kagan and Jackson (2000) and Kagan (2002a, 2002b) propose such distributions defined by two parameters, β and variants of m_{\max} .

Applying these distributions also allows us to address the problem of evaluating the recurrence period for these large earthquakes. Determining maximum earthquake size either by historical or instrumental observations or by qualitative analogies does not provide such an estimate: a similar earthquake may occur hundreds or tens of thousand years later. But Fig. 1 shows how using statistical distributions of earthquake magnitudes may facilitate such calculations.

As we discussed in Subsections 3.1 and 3.3, the moment conservation principle allows us to determine the upper magnitude parameter quantitatively. In this respect area-specific calculations provide a more precise size evaluation for many tectonic zones and, most impor-

tantly, show that the subduction zones effectively share the same upper magnitude parameter (Kagan, 1997). Corner magnitude estimates based on moment conservation are still annoyingly imprecise, with estimates in the range of 8.5 to 9.7. The fact that several subduction zones have been hit with giant earthquakes in the last 110 years suggests that all such zones could experience earthquakes with the corner magnitude towards the top end of that range.

Boundary-specific calculations are not yet as accurate and reliable as the area-specific, and the computation for several subduction zones has not been performed. However, even the approximate estimates in Subsection 3.3 suggest that $m \geq 9$ is an appropriate earthquake size for the Tohoku area.

The seismic moment-frequency relation (Fig. 1 and Table 1) which is based on earthquake statistics for moderate events and the estimate of the corner moment by the moment conservation principle, implies that the return time of magnitude 9 or larger earthquakes off Tohoku is in the range 300 to 400 years. Uchida and Matsuzawa (2011) suggest a recurrence interval of 260-880 years for the $m9$ events. Simons *et al.* (2011) propose a 500-1,000 year interval based in part on the historic record.

Is our estimated recurrence time of 300 to 400 years, based on instrumentally recorded earthquakes and tectonic strain rates, consistent with the historic record of magnitude 9 and larger events? In one interpretation, no such earthquake occurred off Tohoku between the Jogan earthquake and tsunami in year 869 (Minoura *et al.*, 2001) and the 2011 Tohoku event. That implies an empty interval of 1142 years. Assuming Poisson recurrence, the probability of an interval that long or longer is 5% for a recurrence time of 382 years. A longer recurrence time could not be rejected with 95% confidence based on the empty interval. Minoura *et al.* suggested that there may have been three Tohoku-sized tsunamis in the last 3,000 years before 2001. Again assuming Poisson recurrence, there is a 5% chance of observing three or fewer events in 3,000 years for a recurrence time of 387 years. Longer recurrence times cannot

be rejected with 95% confidence. The above calculations assume that the observations are complete for 1,142 and 3,000 years, respectively. The sizes of the reported earthquakes are based on tsunami run-up, and it is quite possible for larger earthquakes to have smaller tsunamis. For example, Koketsu and Yokota (2011) suggest that the 1611 Keicho earthquake may have been about as large as the 2011 event. Thus the historic record, based primarily on tsunami data, does not conflict with our recurrence time estimate of 300 – 400 years,

In conclusion, we would like to evaluate the upper magnitude limit for the subduction zones as well as recurrence intervals for such earthquakes. Two upper global estimates can be calculated: for the gamma distribution, we take the values from Table 1 $m_{cg} = 9.36 \pm 0.27$ to get the 95% upper limit $m_{cg} = 9.9$. Bird and Kagan (2004, Table 5) determined for the tapered G-R (TGR) distribution $m_{cm} = 9.58^{+\infty}_{-0.23}$, and the approximate 95% upper limit $m_{cm} = 10.1$. For the sake of simplicity, we take $m_{\max} = 10.0$. Calculations similar to (9) can be made to obtain an approximate estimate for the average inter-earthquake period. From Fig. 1b by Kagan (2002a) one can determine the return period as it differs from the regular G-R law: the gamma distribution cumulative function at m_c is below the G-R line by a factor of about 10. For the TGR distribution the factor is e . Thus, for the gamma distribution, the recurrence time for the global occurrence of the $m \geq 10.0$ earthquake is about 1,750 years; for the TGR distribution this period is about 475 years. Of course, the distributions in these calculations are extrapolated beyond the limit of their parameters' evaluation range. But the above recurrence periods provide a rough idea how big such earthquakes could be and how frequently they might occur worldwide.

According to the same reasoning for the Flinn-Engdahl #19 zone a $m \geq 10.0$ earthquake could repeat in about 9,000 or 32,000 years for the TGR and the gamma distributions, respectively. The rupture length of the m_{10} event can be estimated from Fig. 9: at about 2,100 km it is comparable to the 3,000 km length of zone #19. These long recurrence periods

indicate that it would be difficult to find displacement traces or the tsunami record for these earthquakes in the paleo-seismic or paleo-tsunami investigations which usually extend over the period of a few thousand years (Wesnousky *et al.*, 1984; Nishenko, 1991; Minoura *et al.*, 2001; Grunewald and Stein, 2006). Moreover, since subduction zone faults are mostly offshore, finding their displacement trace is impractical.

5 Conclusions

A magnitude 9 earthquake off Tohoku should not have been a surprise. Since 1997 there has been evidence that subduction zones have indistinguishable b -values and upper magnitude parameters. Four previous subduction zone earthquakes of magnitude 9 or larger around the globe in the last 110 years should have served as warning. Under reasonable assumptions of plate boundary properties, earthquakes at least as large as 8.5 are required to satisfy the geodetically and geologically observed moment rates. The seismic gap/characteristic earthquakes model, which formed the basis for smaller magnitude limits, was shown to be inadequate as early as 1991.

Recent research, including observations of large earthquakes, geodetic deformation measurements, and numerical modeling have raised the lower limits of the upper magnitude parameters in subduction zones and confirmed that all major subduction zones have essentially equal b -values and upper magnitude parameters. As magnitude records are broken in individual subduction zones, the observed peak magnitudes are approaching the corner magnitudes estimated from moment conservation.

Moment conservation implies that the corner magnitude of subduction zones, taken as a group, should be well above magnitude 9. Given that subduction zones have statistically indistinguishable parameters, magnitude 9 earthquakes can be expected in any major sub-

duction zone. The global rate of magnitude 9 earthquakes, both predicted from statistics of moderate events and from moment conservation and observed during the last 110 years, is about 5 per century.

While earthquakes with a tapered form of Gutenberg-Richter distribution and a corner magnitude of 9.6 would explain observed tectonic deformation at plate boundaries, reasonable models allow for even larger earthquakes. Magnitude 10 earthquakes cannot be considered impossible, and our models suggest a global recurrence time of a few hundred or thousand years.

6 Data and Resources

The global CMT catalog of moment tensor inversions compiled by the GCMT group is available at <http://www.globalcmt.org/CMTfiles.html> (last accessed December 2011). The Centennial catalog by Engdahl and Villaseñor (2002) is available at <http://earthquake.usgs.gov/research/data/centennial.pdf> (last accessed December 2011). Flinn-Engdahl Regions are explained and their coordinates as well as FORTRAN files to process them are available at

http://earthquake.usgs.gov/learn/topics/flinn_engdahl_list/
ftp://hazards.cr.usgs.gov/feregion/fe_1995/ (last accessed December 2011). *Seismic Activity in Japan* Web site

<http://www.jishin.go.jp/main/index-e.html> (last accessed December 2011).

in the Knowledge section see items: ‘Evaluation of Major Subduction-zone Earthquake;’ and ‘Probabilistic seismic Hazard map;’. Also see

<http://go.nature.com/yw5e92> (last accessed May 2012).

Acknowledgments

We are grateful to Peter Bird and Paul Davis of UCLA as well as Robert Geller and Satoshi Ide of the Tokyo University for useful discussion and suggestions. We thank Kathleen Jackson who edited the manuscript. Reviews by Seth Stein and Ross Stein as well as comments by the Associate Editor Thorne Lay have been helpful in revising the manuscript. The authors appreciate partial support from the National Science Foundation through grants EAR-0711515, EAR-0944218, and EAR-1045876, as well as from the Southern California Earthquake Center (SCEC). SCEC is funded by NSF Cooperative Agreement EAR-0529922 and USGS Cooperative Agreement 07HQAG0008. Publication 0000, SCEC.

REFERENCES

- Anderson, J. G., 1979. Estimating the seismicity from geological structure for seismic risk studies, *Bull. Seismol. Soc. Amer.*, **69**, 135-158.
- Annaka, T., Satake, K., Sakakiyama, T., Yanagisawa, K., and Shuto, N. (2007), Logic-tree approach for probabilistic tsunami hazard analysis and its applications to the Japanese coasts, *Pure Appl. Geophys.*, **164**, 577-592.
- Bateman, H., and Erdelyi, A., 1953. *Higher Transcendental Functions*, McGraw-Hill Co., NY.
- Bird, P., 2010. Can diligent and extensive mapping of faults provide reliable estimates of the expected maximum earthquakes at these faults? No. AGU Fall Meet. Abstract S23B-02.
- Bird, P., and Y. Y. Kagan, 2004. Plate-tectonic analysis of shallow seismicity: apparent boundary width, beta, corner magnitude, coupled lithosphere thickness, and coupling in seven tectonic settings, *Bull. Seismol. Soc. Amer.*, **94**(6), 2380-2399, (plus electronic supplement), see also an update at http://peterbird.name/publications/2004_global_coupling/2004_global_coupling.pdf
- Brune, J. N., 1968. Seismic moment, seismicity, and rate of slip along major fault zones, *J. Geophys. Res.*, **73**, 777-784.
- Ekström, G., 2007. Global seismicity: results from systematic waveform analyses, 1976-2005, in *Treatise on Geophysics*, **4**(4.16), ed. H. Kanamori, pp. 473-481, Elsevier, Amsterdam.
- Ekström, G., A. M. Dziewonski, N. N. Maternovskaya and M. Nettles, 2005. Global seismicity of 2003: Centroid-moment-tensor solutions for 1087 earthquakes, *Phys. Earth planet. Inter.*, **148**(2-4), 327-351.
- Engdahl, E.R. and Villaseñor, A., 2002. Global seismicity: 1900-1999, in *IASPEI Handbook*

- of Earthquake and Engineering Seismology*, W. H. K. Lee, H. Kanamori, P. C. Jennings, and C. Kisslinger, Eds., **part A**, pp. 665-690, Boston, Academic Press, available at <http://earthquake.usgs.gov/research/data/centennial.pdf>.
- Fialko, Y., Sandwell, D., Simons, M. and Rosen, P., 2005. Three-dimensional deformation caused by the Bam, Iran, earthquake and the origin of shallow slip deficit, *Nature*, **435**, 295-299, doi:10.1038/nature03425.
- Flinn, E. A., E. R. Engdahl, and A. R. Hill, 1974. Seismic and geographical regionalization, *Bull. Seismol. Soc. Amer.*, **64**, 771-992.
- Geller, R. J., 2011. Shake-up time for Japanese seismology, *Nature*, **472**(7344), 407-409, DOI: doi:10.1038/nature10105.
- Grunewald, E. D. and R. S. Stein, 2006. A new 1649-1884 catalog of destructive earthquakes near Tokyo and implications for the long-term seismic process, *J. Geophys. Res.*, **111**, B12306, doi:10.1029/2005JB004059.
- Gutenberg, B., and C. F. Richter, 1954. *Seismicity of the Earth and Associated Phenomena*, Princeton, Princeton Univ. Press., 310 pp.
- Hanks, T.C., 1992. Small earthquakes, tectonic forces, *Science*, **256**, 1430-1432.
- Hayes, G. P., P. S. Earle, H. M. Benz, D. J. Wald, and R. W. Briggs the USGS/NEIC Earthquake Response Team, 2011. 88 Hours: The U.S. Geological Survey National Earthquake Information Center Response to the 11 March 2011 Mw 9.0 Tohoku Earthquake, *Seismol. Res. Lett.*, **82**(4), 481-493.
- Headquarters for Earthquake Research Promotion, 2005. National Seismic Hazard Maps for Japan available at <http://go.nature.com/yw5e92>, also at <http://www.jishin.go.jp/main/index-e.html> (see Knowledge – Probabilistic seismic Hazard map PDF 2,018 KB)
- Jackson, D. D., and Y. Y. Kagan, 2011. Characteristic earthquakes and seismic gaps, In *Encyclopedia of Solid Earth Geophysics*, Gupta, H. K. (Ed.), Springer, pp. 37-40, DOI

10.1007/978-90-481-8702-7.

- Kagan, Y. Y., 1997. Seismic moment-frequency relation for shallow earthquakes: Regional comparison, *J. Geophys. Res.*, **102**(B2), 2835-2852.
- Kagan, Y. Y., 2002a. Seismic moment distribution revisited: I. Statistical results, *Geophys. J. Int.*, **148**(3), 520-541.
- Kagan, Y. Y., 2002b. Seismic moment distribution revisited: II. Moment conservation principle, *Geophys. J. Int.*, **149**(3), 731-754.
- Kagan, Y. Y., 2002c. Aftershock zone scaling, *Bull. Seismol. Soc. Amer.*, **92**(2), 641-655, doi: 10.1785/0120010172.
- Kagan, Y. Y., 2005. Earthquake slip distribution: A statistical model, *J. Geophys. Res.*, **110**(B5), B05S11, doi:10.1029/2004JB003280, pp. 1-15 (with electronic Appendices).
- Kagan, Y. Y., P. Bird, and D. D. Jackson, 2010. Earthquake patterns in diverse tectonic zones of the globe, *Pure Appl. Geoph. (The Frank Evison Volume)*, **167**(6/7), 721-741, doi: 10.1007/s00024-010-0075-3.
- Kagan, Y. Y., and D. D. Jackson, 1991. Seismic gap hypothesis: ten years after, *J. Geophys. Res.*, **96**, 21,419-21,431.
- Kagan, Y. Y. and D. D. Jackson, 1999. Worldwide doublets of large shallow earthquakes, *Bull. Seismol. Soc. Amer.*, **89**(5), 1147-1155.
- Kagan, Y. Y., and D. D. Jackson, 2000. Probabilistic forecasting of earthquakes, *Geophys. J. Int.*, **143**, 438-453.
- Kagan, Y. Y. and Jackson, D. D., 2012. Long- and short-term earthquake forecasts during the Tohoku sequence, manuscript, submitted to *Earth, Planets and Space (EPS)*, EPS 2011/12/27, EPS3360TH2, preprint <http://arxiv.org/abs/1201.1659>
- Kaneko, Y. and Y. Fialko, 2011. Shallow slip deficit due to large strike-slip earthquakes

- in dynamic rupture simulations with elasto-plastic off-fault response, *Geophys. J. Int.*, **186**, 1389-1403, doi: 10.1111/j.1365-246X.2011.05117.x
- Koketsu, K., and Y. Yokota, 2011. Supercycles along the Japan Trench and Foreseeability of the 2011 Tohoku Earthquake, AGU Fall Meet. Abstract U33C-03.
- Koravos, G.C., Tsapanos, T.M., and Bejaichund, M., 2006. Probabilistic seismic hazard assessment for Japan, *Pure Appl. Geophys.*, **163**(1), 137-151, DOI: 10.1007/s00024-005-0003-0
- Manighetti, I., Campillo, M., Sammis, C., Mai, P.M., and King, G., 2005. Evidence for self-similar, triangular slip distributions on earthquakes: Implications for earthquake and fault mechanics, *J. Geophys. Res.*, **110**(B5), B05302.
- Manighetti, I., Zigone, D., Campillo, M., and Cotton, F., 2009. Self-similarity of the largest-scale segmentation of the faults: Implications for earthquake behavior, *Earth Planet. Sci. Lett.*, **288**(3-4), 370-381.
- Matthews, M. V., W. L. Ellsworth, and P. A. Reasenberg, 2002. A Brownian model for recurrent earthquakes, *Bull. Seismol. Soc. Amer.*, **92**, 2233-2250.
- McCaffrey, R., 2007. The Next Great Earthquake, *Science*, **315**, 1675, DOI: 10.1126/science.1140173
- McCaffrey, R., 2008. Global frequency of magnitude 9 earthquakes, *Geology*, **36**(3), 263-266, DOI: 10.1130/G24402A.1 (GSA Data Repository item 2008063, Table DR1).
- McGuire, J. J., and G. C. Beroza, 2012. A Rogue Earthquake Off Sumatra, *Science*, **336**(6085), 1118-1119, DOI: 10.1126/science.1223983.
- Michael, A. J., 2011. Random variability explains apparent global clustering of large earthquakes, *Geophys. Res. Lett.*, **38**, L21301, doi:10.1029/2011GL049443.
- Minoura, K., F. Imamura, D. Sugawara, Y. Kono, and T. Iwashita, 2001. The 869 Jogan

- tsunami deposit and recurrence interval of large-scale tsunami on the Pacific coast of northeast Japan, *J. Natural Disaster Sci.*, **23**, 83-88.
- Molnar, P., 1979. Earthquake recurrence intervals and plate tectonics, *Bull. Seismol. Soc. Amer.*, **69**, 115-133.
- Nanjo, K. Z., H. Tsuruoka, N. Hirata, and T. H. Jordan, 2011. Overview of the first earthquake forecast testing experiment in Japan, *Earth Planets Space*, **63**(3), 159-169.
- Nettles, M., Ekström, G., and H. C. Koss, 2011. Centroid-moment-tensor analysis of the 2011 off the Pacific coast of Tohoku Earthquake and its larger foreshocks and aftershocks, *Earth Planets Space*, **63**(7), 519-523.
- Nishenko, S. P., 1991. Circum-Pacific seismic potential – 1989-1999, *Pure Appl. Geophys.*, **135**, 169-259.
- Ozawa, S., T. Nishimura, H. Suito, T. Kobayashi, M. Tobita, and T. Imakiire, 2011. Co-seismic and postseismic slip of the 2011 magnitude-9 Tohoku-Oki earthquake, *Nature*, **475**, 373-376, DOI: doi:10.1038/nature10227
- Rikitake, T. and I. Aida (1988). Tsunami hazard probability in Japan, *Bull. Seismol. Soc. Amer.*, **78**, 1268-1278.
- Ruff, L., and H. Kanamori, 1980. Seismicity and the subduction process, *Phys. Earth Planet. Inter.*, **23**, 240-252.
- Seismic Activity in Japan, 2008. <http://www.jishin.go.jp/main/index-e.html>, see the Knowledge section.
- Shaw, B. E., and S. G. Wesnousky, 2008. Slip-length scaling in large earthquakes: the role of deep-penetrating slip below the seismogenic layer, *Bull. Seismol. Soc. Amer.*, **98**(4), 1633-1641.
- Simons, M., Minson, S.E., Sladen, A., Ortega, F., Jiang, J.L., Owen, S.E., Meng, L.S.,

- Ampuero, J.P., Wei, S.J., Chu, R.S., Helmberger, D.V., Kanamori, H., Hetland, E., Moore, A.W., and Webb, F.H., 2011. The 2011 magnitude 9.0 Tohoku-Oki earthquake: mosaicking the megathrust from seconds to centuries, *Science*, **332**(6036), 1421-1425 DOI: 10.1126/science.1206731.
- Stein, S., Geller, R., and Liu, M., 2011. Bad assumptions or bad luck: why earthquake hazard maps need objective testing, *Seismol. Res. Lett.*, **82**(5), 623-626.
- Stein, S., and E. A. Okal, 2007. Ultralong Period Seismic Study of the December 2004 Indian Ocean Earthquake and Implications for Regional Tectonics and the Subduction Process, *Bull. Seismol. Soc. Amer.*, **97**(1A), S279-S295
- Stein, S., and E. A. Okal, 2011. The size of the 2011 Tohoku earthquake need not have been a surprise, *Eos Trans. AGU*, **92**(27), 227-228.
- Sugawara, D., F. Imamura, K. Goto, H. Matsumoto, and K. Minoura, 2012. The 2011 Tohoku-oki Earthquake Tsunami: Similarities and Differences to the 869 Jogan Tsunami on the Sendai Plain, *Pure Appl. Geophys.*, DOI 10.1007/s00024-012-0460-1.
- Uchida, N., and T. Matsuzawa, 2011. Coupling coefficient, hierarchical structure, and earthquake cycle for the source area of the 2011 off the Pacific coast of Tohoku earthquake inferred from small repeating earthquake data, *Earth Planets Space*, **63**(7), 675-679.
- Wesnousky, S. G., C. H. Scholz, K. Shimazaki, and T. Matsuda, 1984. Integration of geological and seismological data for the analysis of seismic hazard: a case study of Japan, *Bull. Seismol. Soc. Amer.*, **74**, 687-708.
- Wyss, M., 1973. Towards a physical understanding of the earthquake frequency distribution, *Geophys. J. R. Astr. Soc.*, **31**, 341-359.
- Young, J. B., B. W. Presgrave, H. Aichele, D. A. Wiens, and E. A. Flinn, 1996. The Flinn-Engdahl regionalisation scheme: the 1995 revision, *Phys. Earth Planet. Inter.*,

96, 223-297.

Zaliapin, I. V., Y. Y. Kagan, and F. Schoenberg, 2005. Approximating the distribution of Pareto sums, *Pure Appl. Geoph.*, **162**(6-7), 1187-1228.

Table 1: FE Subduction Seismic Zones, GCMT 1977-2010/12/31, $m_t = 5.8$.

FE		Flinn-Engdahl			\dot{M}_T		\dot{M}_s		
No	No	seismic region name	N	$\beta \pm \sigma_\beta$	$\times 10^{27}$	$m_c \pm \sigma_M$	m_o	$\times 10^{27}$	ψ
1	1	Alaska-Aleutian Arc	280	0.65±0.04	5.10	9.35±0.28	8.0	1.71	0.336
2	5	Mexico-Guatemala	164	0.60±0.06	2.38	9.17±0.29	8.0	1.35	0.567
3	6	Central America	161	0.68±0.06	2.49	9.22±0.29	7.8	0.59	0.236
4	7	Caribbean Loop	59	0.62±0.09	1.05	9.33±0.31	7.4	0.13	0.125
5	8	Andean S. America	286	0.57±0.04	8.49	9.74±0.28	8.8	9.54	1.124
6	12	Kermadec-Tonga-Samoa	439	0.80±0.04	5.95	9.12±0.28	8.1	2.16	0.363
7	13	Fiji Is	79	0.85±0.10	2.29	9.72±0.30	6.8	0.06	0.026
8	14	New Hebrides Is	424	0.59±0.03	4.81	8.98±0.28	7.9	1.76	0.366
9	15	Bismarck-Solomon Is	448	0.60±0.03	4.93	8.95±0.28	8.1	2.46	0.500
10	16	New Guinea	266	0.66±0.05	8.49	9.80±0.28	8.3	1.48	0.174
11	18	Guam-Japan	88	0.86±0.10	2.89	9.82±0.30	7.8	0.34	0.117
12	19	Japan-Kamchatka	425	0.62±0.04	8.49	9.43±0.28	8.4	5.30	0.624
12a	–	Tohoku area ($5^\circ \times 6^\circ$)	109	0.64±0.07	1.76	9.26±0.29	7.7	0.32	0.180
13	20	S.E. Japan-Ryukyu Is	57	0.62±0.10	1.81	9.79±0.31	7.2	0.10	0.054
14	21	Taiwan	110	0.64±0.07	1.53	9.14±0.29	7.7	0.35	0.226
15	22	Philippines	244	0.68±0.05	3.54	9.17±0.28	7.7	0.74	0.208
16	23	Borneo-Celebes	266	0.68±0.05	4.16	9.23±0.28	7.9	1.09	0.261
17	24	Sunda Arc	278	0.65±0.04	6.51	9.55±0.28	8.6	4.66	0.716
18	46	Andaman Is-Sumatra	143	0.71±0.07	2.66	9.37±0.29	9.1	15.26	5.734
1977-2010/12/31 ZONES			4217	0.65±0.01	77.57	9.36±0.27	9.1	49.07	0.633
1977-1995/6/30 ZONES			2127	0.63±0.02	27.40	8.60±0.27	8.4	20.67	0.754

Notes: FE – Flinn-Engdahl seismic region; W – seismogenic width, μ – elastic shear modulus, χ – seismic coupling coefficient, N – earthquake number, β – parameter of the power-law distribution of earthquake sizes, \dot{M}_T – annual tectonic moment rate, \dot{M}_s – annual seismic moment rate, m_c – corner magnitude; m_o – maximum moment magnitude observed in 1977-2010, $\psi = \dot{M}_s/\dot{M}_T$ – ratio of seismic to tectonic moment rate. Seismic moment and moment rate are measured in *dyne-cm* and *dyne-cm/yr*, respectively. Tectonic rate for 1977-2010/12/31 period is calculated by using Bird and Kagan (2004) parameters: $W = 104$ km, $\mu = 49$ GPa, $\chi = 0.5$. In the last line of the Table we show the subduction zones total calculation results for Kagan (1997, Table 1), where the following parameters have been used: $W = 30$ km, $\mu = 30$ GPa, $\chi = 1.0$.

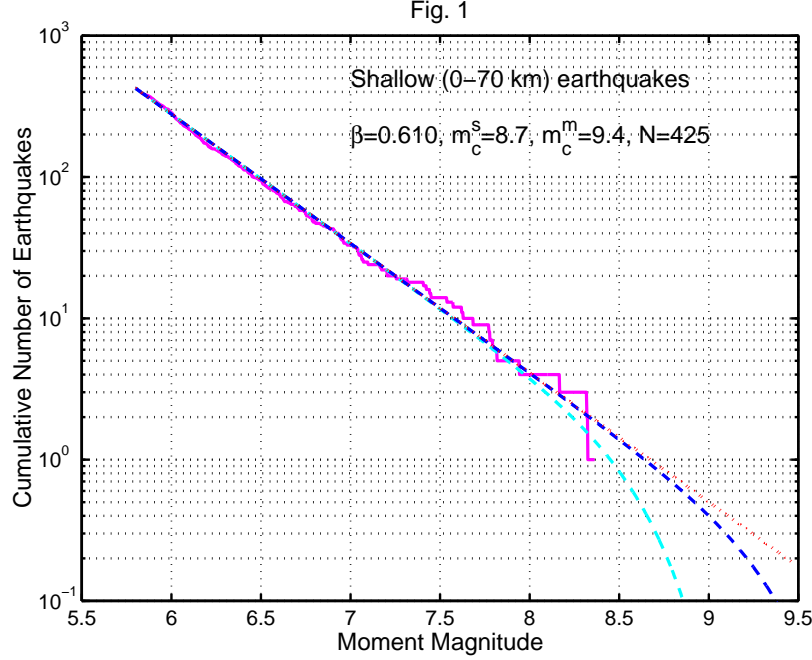


Figure 1:

Solid line – the number of earthquakes in the Flinn-Engdahl zone #19 (Japan–Kurile–Kamchatka) with the moment magnitude (m) larger than or equal to m as a function of m for the shallow earthquakes in the GCMT catalog during 1977–2010. Magnitude threshold $m_t = 5.8$, the total number of events is 425. The unrestricted Gutenberg-Richter law is shown by a dotted line (Kagan, 2002a). Dashed lines show two tapered G-R (TGR) distributions: the G-R law restricted at large magnitudes by an exponential taper with a corner magnitude. Left-hand line is for the corner magnitude $m_c^s = 8.7$ evaluated by the maximum likelihood method using the earthquake statistical record (with no upper limit, see Fig. 2). Right-hand line is for the corner moment estimate $m_c^m = 9.4$ is based on the moment conservation (see Table 1). The slope of the linear part of the curves corresponds to $\beta = 0.610$.

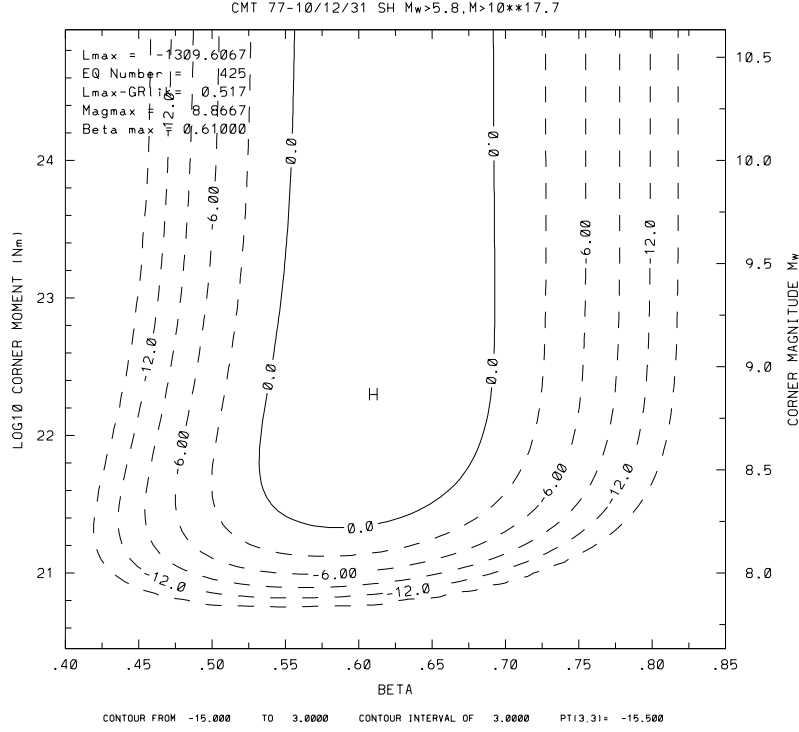


Figure 2:

A log-likelihood map for the distribution of the scalar seismic moment of earthquakes in the Flinn-Engdahl zone #19 (Japan–Kurile–Kamchatka): the GCMT catalog time span is 1977/1/1–2010/12/31; the seismic moment cutoff is $10^{17.7}$ Nm ($m_t = 5.8$); the number of events is 425. The approximation by the gamma distribution. The ‘H’ sign indicates the map maximum; the value of the function is adjusted to be 3.0 at this place. The zero contour (the solid line) corresponds to the 95% confidence area (Kagan, 1997).

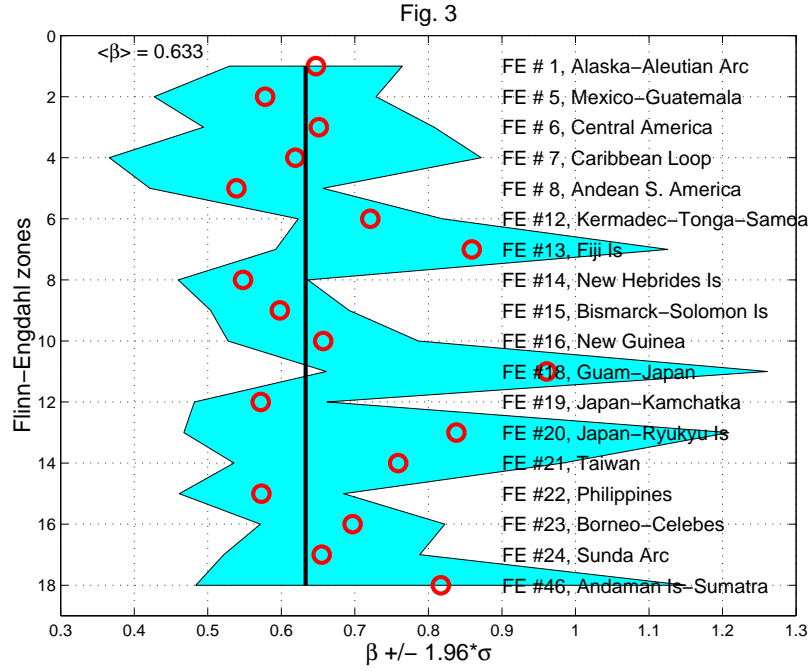


Figure 3:

Parameter β distribution in the Flinn-Engdahl (FE) subduction zones; average β -values are shown by circles. GCMT catalog 1977-1995/6/30. The ordinate numbers are sequential numbers of subduction zones considered, the FE numbers and names for these zones are shown in the right-hand part of the diagram. Average region's β and ± 1.96 standard deviations are shown; the solid line corresponds to the average $\langle \beta \rangle = 0.633$ for all subduction zones.

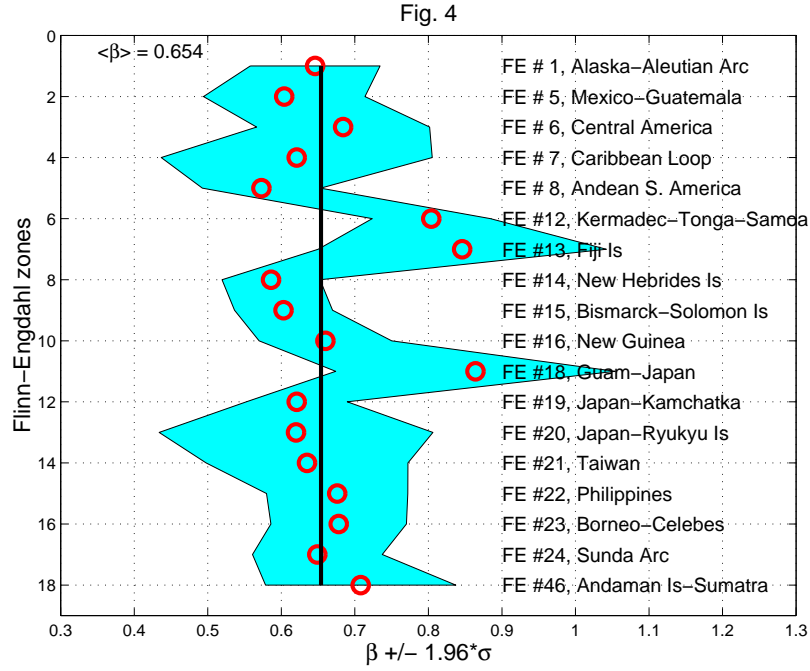


Figure 4:

Parameter β distribution in Flinn-Engdahl subduction zones. GCMT catalog 1977-2010.

The average $\langle \beta \rangle = 0.654$ for all subduction zones. For notation see Fig. 3.

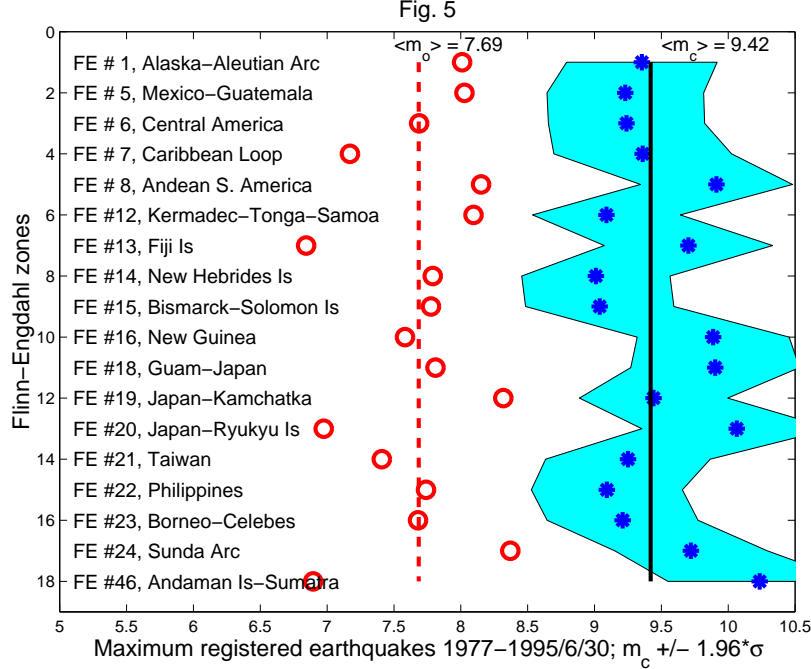


Figure 5:

The corner moment magnitude m_c distribution in the Flinn-Engdahl subduction zones. GCMT catalog 1977-1995/6/30. The region's m_c and ± 1.96 standard deviations are shown. The solid line corresponds to the average $\langle m_c \rangle = 9.42$ for all subduction zones. In m_c calculations (Eq. 7) we use the parameters of the tectonic motion as proposed by Bird and Kagan (2004): $W = 104$ km, $\mu = 49$ GPa, $\chi = 0.5$. Circles show events with the maximum magnitude m_o in the regions during the catalog time interval. The dashed line corresponds to the average $\langle m_o \rangle = 7.69$ for all subduction zones.

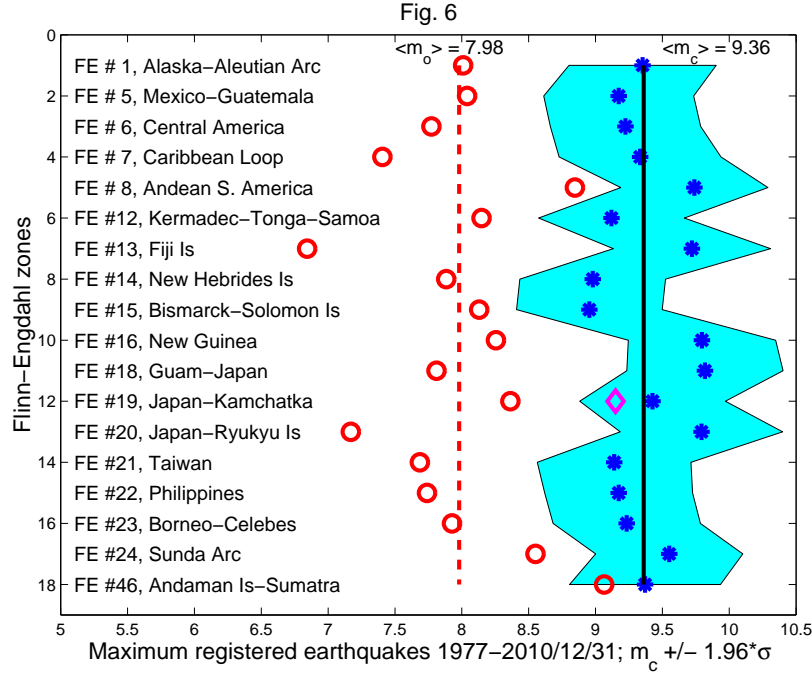


Figure 6:

The corner moment magnitude m_c distribution in the Flinn-Engdahl subduction zones. GCMT catalog 1977-2010. Averages of the corner magnitude ($\langle m_c \rangle = 9.36$) and the maximum observed magnitude ($\langle m_o \rangle = 7.98$) for all subduction zones are shown. Diamond shows the Tohoku mega-earthquake magnitude. For notation see Fig. 5.

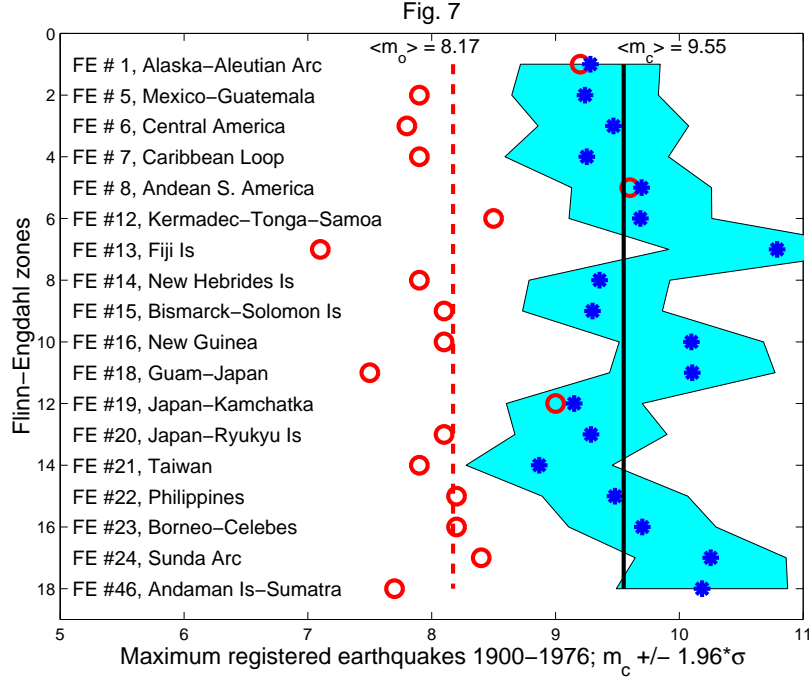


Figure 7:

The corner moment magnitude m_c distribution in the Flinn-Engdahl subduction zones, using the Centennial catalog, 1900-1976, with magnitude threshold $m_t = 6.5$. Averages $\langle m_c \rangle = 9.55$ and $\langle m_o \rangle = 8.17$ for all subduction zones. For notation see Fig. 5.

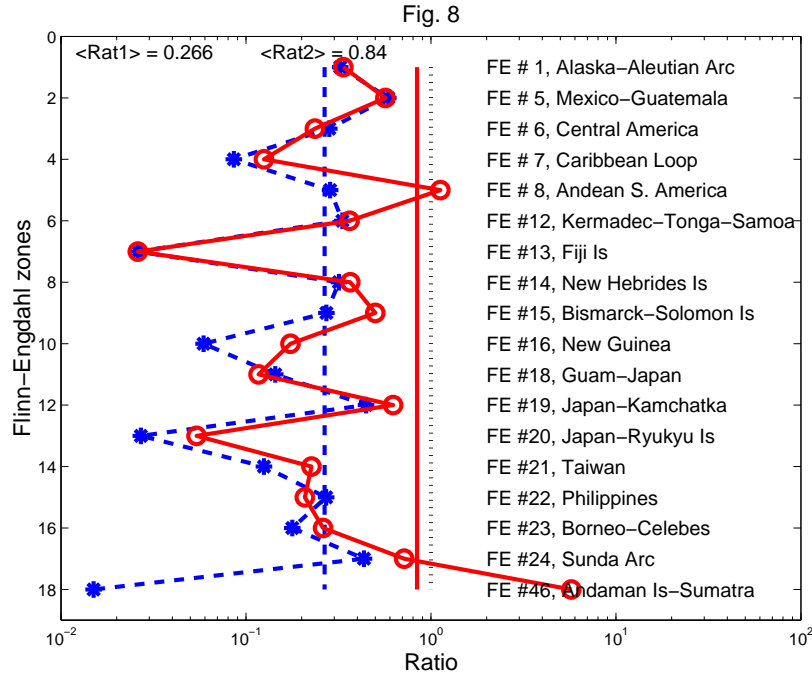


Figure 8:

Ratio (ψ) of the seismic to tectonic rate in the Flinn-Engdahl subduction zones for the GCMT catalog 1977-1995/6/30 (dashed lines) and 1977-2010 (solid lines). Vertical lines show the average ratio for all regions ($\psi_1 = 0.266$; $\psi_2 = 0.84$); the dotted line corresponds to the ratio of 1.0. See also the last column of Table 1.

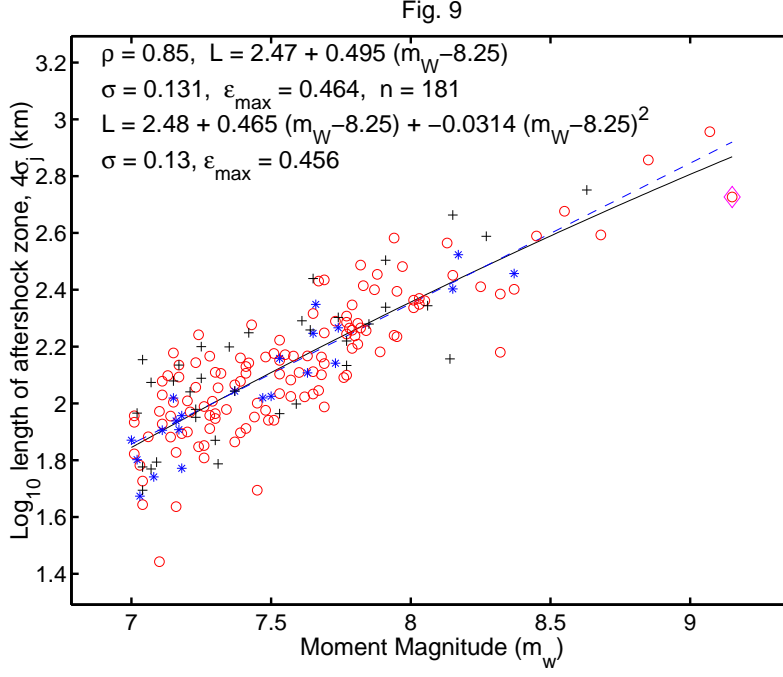


Figure 9:

The plot of the log aftershock zone length (L) against the moment magnitude (m). Earthquakes 1977-2012/04 are used. The rupture length is determined using a 1-day aftershock pattern. The values of the correlation coefficient (ρ), coefficients for linear (dashed line) and quadratic (solid line) regression, standard (σ) and maximum (ϵ_{\max}) errors, and the total number (n) of aftershock sequences are shown in the diagram. Both lines for the linear regression and the quadratic approximation practically overlap in the plot.

Circles – thrust mainshocks;

Stars – normal mainshocks;

Pluses – strike-slip mainshocks.

The Tohoku mega-earthquake is marked by a diamond sign.